Journal of Alloys and Compounds 509 (2011) 5810–5815

Contents lists available at ScienceDirect

Journal of Alloys and Compounds

journal homepage: www.elsevier.com/locate/jallcom

Effects of sputtering pressure and post-metallization annealing on the physical properties of rf-sputtered Y_2O_3 films

Z. Yu, L.Y. Liang, Z.M. Liu, W.Y. Xu, X.L. Sun, H.T. Cao*

Ningbo Institute of Materials Technology and Engineering (NIMTE), Chinese Academy of Sciences (CAS), Ningbo 315201, PR China

ARTICLE INFO

Article history:
Received 15 November 2010
Received in revised form 21 February 2011
Accepted 22 February 2011
Available online 1 March 2011

Keywords:
Y_2O_3 dielectric films
Reactive rf-sputtering
Post-metallization annealing
Leakage current

ABSTRACT

Y_2O_3 thin films were prepared by rf-sputtering under various sputtering pressures at room temperature. Spectroscopic ellipsometer, X-ray diffraction and semiconductor parameter analyzer were used to characterize the studied films. The results show the crystallinity and leakage current density of the films improved with decreasing sputtering pressure. The effects of post-metallization annealing (PMA) on optical, structural and electrical properties of the films were also evaluated. It is found that PMA can significantly enhance the electrical performance of Y_2O_3 film, and the lowest leakage current is found to be 1.54×10^{-8} A/cm^2 at 1 MV/cm for the samples treated at 350 °C for 30 min. The leakage current mechanisms were discussed as well, which reveals that space charge limited current dominates the as-deposited films while Schottky mechanism describes the PMA treated ones well.

1. Introduction

With the ever increasing need for higher speed and lower power consumption device pushed the amorphous Si-based TFT to its performance limit, transparent thin-film transistors (TTFTs) have attracted considerable attentions for the use in active-matrix liquid crystal displays (AMLCD), and TTFTs basically provide two principal advantages over Si-TFT: less thermal consumption and lower cost [1–4]. As a key element in TTFT, qualified high permittivity (high-k) dielectrics determine the performance of the device. The TTFT research community are now looking for such dielectrics to be able to modulate enough charges under a practical gate bias, as well as to realize large area and low temperature fabrication. So far, the intensively investigated high-k materials include transition metal (TM) oxides (HfO_2, Y_2O_3, Ta_2O_5, etc.) and their alloys. Among them, Y_2O_3 has been considered as a promising candidate for the characteristic of wide band-gap (5.5–6 eV), relatively high dielectric constant (14–18), good thermodynamic stability (up to 2325 °C), and the easy availability in large areas [5–8].

The reactive radio frequency magnetron sputtering (rf-sputtering) technique is widely used to fabricate thin films. Its stable procedure and easy-controllability guarantee the large scale manufacture [9–11]. The structural, opto-electrical properties of sputtered films are closely related to the sputtering parameters. One of those is sputtering pressure and it is controlled by the flux of sputtering gas. The change of pressure inside the discharge chamber can alter the probability of mutual collision between discharge ions and sputtered particles, which would greatly affect the mean free path of the sputtered particles and eventually the film quality. Besides in situ parameters, *ex situ* treatments also influence the quality of sputtered films, among which post-metallization annealing (PMA) is an effective method to polish the properties of both materials and devices [12,13]. More specifically, the low-temperature post-metallization annealing process has been regarded as a useful procedure in metal-oxide-semiconductor (MOS) technology to reduce the interface trap density by passivating and repairing oxide-related trap charge [15].

In this work, we concentrate on the effects of sputtering pressure and low temperature PMA treatment on the optical, structural and electrical properties of Y_2O_3 dielectric films.

2. Experimental

Prior to the deposition of Y_2O_3 films, both the surface of ITO glass and Si substrate were cleaned with acetone, methanol, and deionized water, in that order. The Y_2O_3 films were prepared by reactive rf-magnetron sputtering from a 2-in. yttrium metallic target (4 N) in a high vacuum chamber under a base pressure of around 5×10^{-5} Pa. Distance between substrate and the target is 14.5 cm. Before sputtering, the substrate surface was cleaned by Ar^+ bombardment for 5 min in order to further reduce contaminations, and pre-sputtering was carried out in pure Ar ambient for 10 min to clean the target surface. The sputtering power was 100 W and the Ar/O_2 gas flow ratio was fixed at 10:1 while total sputtering pressure was adjusted to be 0.33 Pa, 0.27 Pa and 0.22 Pa. In order to obtain a constant film thickness of ~140 nm, deposition time for each sample was varied, depending on the sputtering pressure. After the deposition of dielectric, approximately 200 nm thick Al top electrodes were formed immediately for the fabrication of metal/insulator/metal (MIM) capacitors using a conventional dc-sputtering in Ar ambient through a shadow mask with a circular contact area of 3.14×10^{-4} cm^2. The samples with optimal overall perfor-

* Corresponding author. Tel.: +86 574 8668 5161; fax: +86 574 8668 5163.
E-mail address: h.cao@nimte.ac.cn (H.T. Cao).

0925-8388/$ – see front matter.
doi:10.1016/j.jallcom.2011.02.127

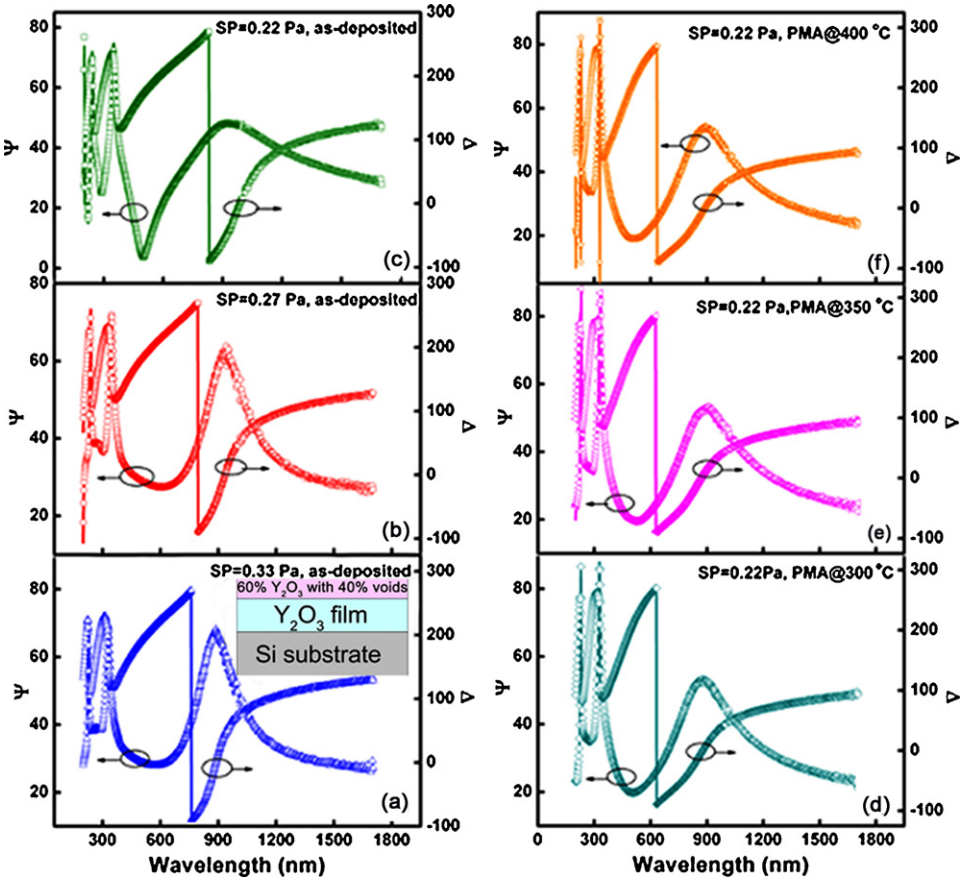

Fig. 1. Experimental (dots) and fitted (solid lines) SE data for samples (a) sputtering pressure (SP) = 0.33 Pa, as-deposited; (b) SP = 0.27 Pa, as-deposited; (c) SP = 0.22 Pa, as-deposited; (d) SP = 0.22 Pa, 300 °C PMA; (e) SP = 0.22 Pa, 350 °C PMA; (f) SP = 0.22 Pa, 400 °C PMA. Inset is the schematic structure of the optical model.

mance under a sputtering pressure of 0.22 Pa were processed in 300 °C for 30 min, 350 °C for 1 min, 10 min, 30 min and 50 min, and 400 °C for 30 min, respectively, to further study the influence of PMA treatment.

The thickness and optical properties of Y_2O_3 films were determined *ex situ* using a spectroscopic ellipsometer (SE) (J.A. Woollam Co., Inc., M-2000DI). The ellipsometric angle ψ and phase difference Δ were recorded ranging from 200 nm to 1700 nm at incidence angles of 55°, 65°, and 75°. The structures of Y_2O_3 films were investigated by X-ray diffraction (XRD) using a Brucker D8 Advance X-ray diffractometer. The electrical characteristics of Y_2O_3 films were measured by using a semiconductor parameter analyzer (Keithley 4200-scs) in the dark at room temperature.

3. Results and discussion

3.1. Optical properties

Spectroscopic ellipsometry (SE) is known as a sensitive and nondestructive method to characterize the optical properties of materials. It has been reported that SE data can also provide information about crystallization and densification of the film in terms of the dielectric function [16].

The dependence of refractive index and band gap of Y_2O_3 films on the diverse sputtering pressures and PMA conditions is demonstrated based on the spectroscopic ellipsometry analysis. Assuming Y_2O_3 could hardly react with Si at temperatures lower than 400 °C [17], we used a three-phase model of substrate/Y_2O_3 film/surface roughness layer (60% Y_2O_3 film with 40% voids) to represent our samples, as shown in the inset of Fig. 1. The dielectric function and the optical parameters of the films, such as thickness and refractive index, can be obtained from ellipsometric parameters ψ and Δ. Tauc–Lorentz (TL) dispersion function [18] was adopted to extract the dielectric functions of Y_2O_3 films. The imaginary part (ε_2) of dielectric function is obtained by combining the classical expression of the imaginary part of the dielectric functions above the band edge with the standard TL expression, and the real part (ε_1) of dielectric functions is a result of self-consistent Kramers–Kroig integration of ε_2. The following equations summarize ε_1 and ε_2 as a function of photon energy E:

$$\varepsilon_2(E) = \begin{cases} 0, (E \le E_g) \\ \dfrac{AE_0C(E-E_g)^2}{\left(E^2-{E_0}^2\right)^2 + C^2E^2} \cdot \dfrac{1}{E}, (E \ge E_g) \end{cases} \quad (1)$$

and

$$\varepsilon_1(E) = \varepsilon_\infty + \frac{2}{\pi} P \int_{E_g}^{\infty} \frac{\xi\varepsilon_2(\xi)}{\xi^2 - E^2} d\xi \quad (2)$$

Eqs. (1) and (2) are uniquely defined by five parameters: ε_∞, A (transition matrix element), C (broadening term), E_0 (peak transition energy), and E_g (optical band gap). For each sample, the five TL parameters and dielectric functions are determined by the least-square fitting from the experimental data.

The experimental data (dots) and fitted (solids lines) SE data of ψ and Δ shown in Fig. 1 are in good agreement with each other, which implies the optical parameters of the films are simulated with high precision. Also, the quality of fitted result was assessed by the mean-squared-error (MSE) function, of which the values are always smaller than 10, further assuring the reliability.

Fig. 2 displays the dependence of the refractive index (n) of Y_2O_3 films on the sputtering pressure as a function of photon energy. It is obtained that the n values at 543.5 nm for the samples under a sputtering pressure of 0.33 Pa, 0.27 Pa and 0.22 Pa are 1.80, 1.83 and 1.86, respectively. These values are comparable to those reported for high density Y_2O_3 [19]. Refractive index (n) is closely related to

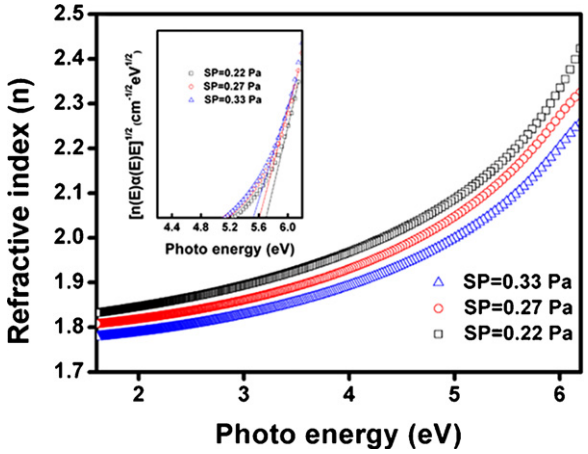

Fig. 2. The dependence of refractive index (n) of Y_2O_3 films on the sputtering pressure as a function of photon energy. Inset is the Tauc plots to determine the band gap.

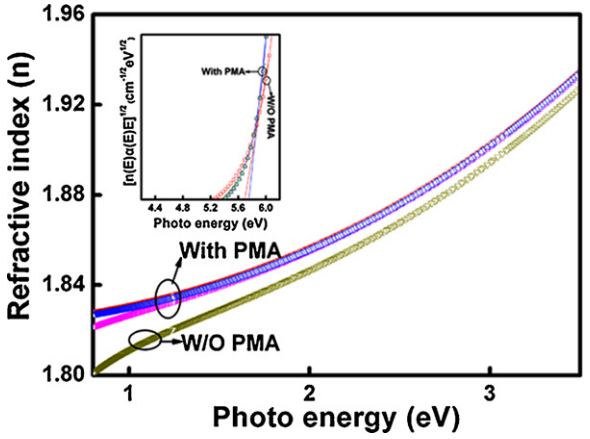

Fig. 3. Plots of refractive index (n) and band gap (inset) for Y_2O_3 films under a sputtering pressure of 0.22 Pa with 300 °C, 350 °C and 400 °C PMA treated or not.

the film density, which can be explained in the terms of the mean free path point. The mean free path of a sputtered particle passing through the deposition chamber before it collides with discharge gas molecules is given by [9]:

$$\lambda_1 = \frac{c_1}{\nu_{12}} \tag{3}$$

where c_1 is the mean velocity of sputtered atoms and ν_{12} is the mean collision frequency between sputtered atoms and discharge gas molecules. Since the velocity of sputtered particles is much larger than the gas molecules, ν_{12} is given by:

$$\nu_{12} = \pi(r_1 + r_2)^2 c_1 * n_2 \tag{4}$$

where r_1 and r_2 are the atomic radii of sputtered atoms and discharge gas molecules, respectively, and n_2 is the density of discharge gas. Then, the mean free path is simply given by:

$$\lambda_1 = \frac{1}{\pi(r_1 + r_2)^2 n_2} \tag{5}$$

From Eq. (5) it is concluded that a longer mean free path is realized by decreasing the sputtering pressure. As it is well known that, atoms with bigger mean free path have higher surface mobility to form a denser film resultantly [20]. Furthermore, Cheng et al. [5] believe that the atomic kinetic energy is dissipated by frequent collision with the ambient gases as pressure increases. So, the low atomic kinetic energy reduces the possibility of adatoms to look for low energy site to reside before covered by the next layer of atoms. Drude equation [21] is introduced to confirm the above analysis, i.e.,

$$1 - p = \frac{n_f^2 - 1}{n_b^2 - 1} \tag{6}$$

where n_f is refractive index of porous materials, n_b the refractive index of bulk materials, and p the mean value of the porosity. The refractive index (n_b) of the bulk Y_2O_3 is 1.936 at 543.5 nm [22]. Based on Eq. (6), the porosity p of the samples under sputtering pressure of 0.33 Pa, 0.27 Pa and 0.22 Pa are calculated to be 19.5%, 15.5% and 10.5%, respectively, confirming that the bigger refractive index, the higher thin film packing density [23,24].

Another factor should be concerned is the optical band gap (E_g) derived from the inverted dielectric functions. A common method to determine E_g is to use Tauc plot, which has already been employed to acquire E_g of Y_2O_3 [22]. As illustrated in the inset of Fig. 2, the band gap E_g is extracted by extrapolating a straight line near the band edge to zero from the plot of $[n(E)\alpha(E)E]^{1/2}$ vs. photon energy (E), where $n(E)$ is the refractive index (n), and $\alpha(E)$ represents absorption coefficient of the film. The obtained band gap displays a slight blue shift from 5.53 to 5.58 then to 5.68 corresponding to the sputtering pressure of 0.33 Pa, 0.27 Pa and 0.22 Pa, respectively. It is believed that the presence of defect and disorder in the film would yield localized states in the band structure which are responsible for the shrink of band gap [22]. Based on the analysis above, the deposited atoms having higher kinetic energy can diffuse more freely on the film surface, which gives rise to reduce the amount of defect and disorder localized in the band structure, to densify the films, and to expand the band gap eventually.

Fig. 3 depicts the refractive index (n) of the sputtered Y_2O_3 films (under a sputtering pressure of 0.22 Pa) with and without PMA treatment. The refractive index (n) of the samples become bigger after PMA treatment, and the mechanism is probably described as follows: the as-deposited films are always in loose arrangement with some voids incorporated during the sputtering, and the annealing procedure can eliminate some voids and activate the atoms to rearrange in the films, which leads to the formation of more closely packed films and correspondingly, the larger refractive index. Kim et al. [25] also proved that low temperature annealing promoted thin film densification rather than cause the interfacial layer growth. This assumption is also confirmed by Drude equation, from which the calculated porosity values for 300 °C, 350 °C and 400 °C PMA treated samples are 9.7%, 9.6% and 9.5%, respectively, while for the as-deposited one, the calculated p is 10.5%.

3.2. Structural properties

It is clearly presented in Fig. 4 that the as-deposited films feature polystalline nature in this study. Both the (2 2 2) and (3 1 0) peaks are weak and broad for the sample under a sputtering pressure of 0.33 Pa, while for the samples under sputtering pressure of 0.27 Pa and 0.22 Pa, the two diffraction peaks become a bit intense, suggesting an improved crystallinity with decreasing sputtering pressure. (2 2 2) Diffraction peak is the strongest in all the samples, indicating that (1 1 1) plane is the preferential orientation of Y_2O_3 films [6] and the sputtered Y_2O_3 films are dominated by (1 1 1) cubic phase [26]. For the samples treated with PMA, the intensity of (2 2 2) peaks enhances significantly, implying that the crystallinity is also getting better after annealing. Moreover, an obvious (4 0 0) diffraction peak appears in the PMA-treated sample, implying that PMA contributes to promote the grain growth. The variation of XRD pattern of the as-deposited Y_2O_3 is consistent to that of optical properties with different pressure. Since the sputtered particles are more eas-

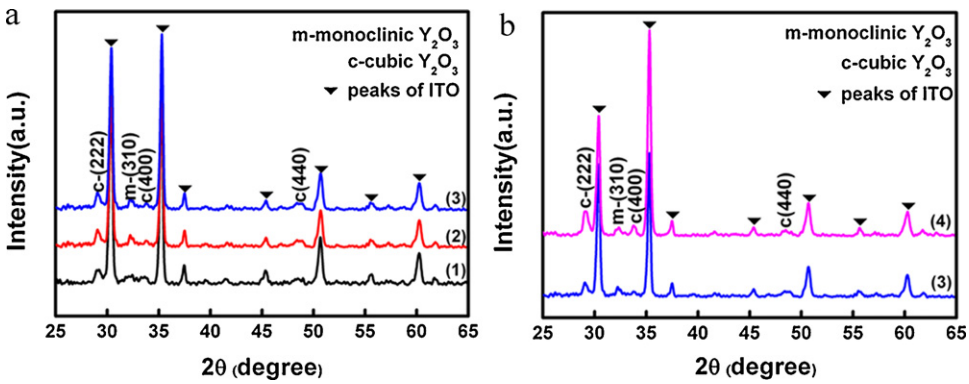

Fig. 4. XRD patterns of Y_2O_3 dielectric/ITO glass substrate (a) as-deposited samples with sputtering pressure of: (1) 0.33 Pa, (2) 0.27 Pa, (3) 0.22 Pa; (b) samples with a sputtering pressure of 0.22 Pa (3) as-deposited, (4) 350 °C/30 min PMA.

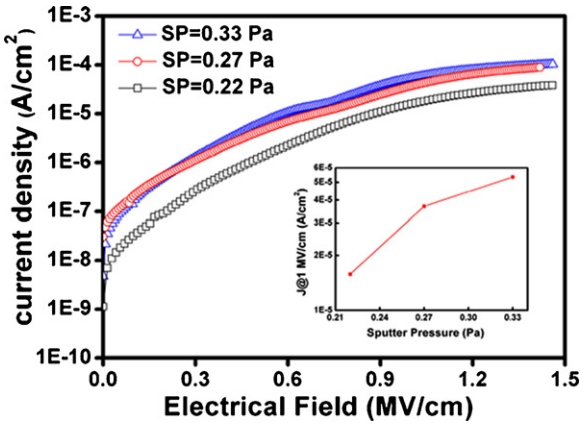

Fig. 5. The *J–E* curves as a function of sputtering pressure. Inset is *J*@1 MV/cm under various sputtering pressure.

ily to collide with each other or with the discharge ions in the case of higher pressures, there are more particles with too low energy to arrive at the substrate, which leads to less intensive diffraction peak [27]. When treated with annealing, on one side, the atoms are activated by heat energy to rearrange in the lattice; on the other, grain size is allowed to grow larger, so the crystallinity is improved consequentially.

3.3. Electrical properties

Fig. 5 represents the leakage current density–applied electric field (*J–E*) characteristics of Al/Y_2O_3/ITO MIM capacitors. The leakage current values at 1 MV/cm are 5.34×10^{-5}, 3.70×10^{-5} and 1.58×10^{-5} A/cm^2 under a sputtering pressure of 0.33 Pa, 0.27 Pa and 0.22 Pa, respectively, revealing that leakage current density gets reduced with decreasing sputtering pressure. In particular, the drop is calculated to be 70.4% from sputtering pressure of 0.33 Pa to 0.22 Pa. The leakage current density is influenced by the film density, crystallinity, and surface morphology [28]. It can be derived from the optical and structural analysis that Y_2O_3 films have larger packing density as well as better crystallinity with decreasing sputtering pressure. Also the surface roughness thickness obtained from SE is 13.3 nm, 12.0 nm and 10.7 nm under a sputtering pressure of 0.33 Pa, 0.27 Pa, and 0.22 Pa, respectively, indicating improved surface morphology with decreasing sputtering pressure [29].

Afterwards, the as-deposited samples under a sputtering pressure of 0.22 Pa were selected to conduct PMA treatments at different temperatures as well as various durations, in order to study the effects of PMA on the electrical performance of Al/Y_2O_3/ITO capacitors, as shown in Fig. 6. The asymmetry of leakage current curves for the top injection and bottom injection mode is due to the asymmetry of ITO bottom electrode and Al top electrode. Although some previous studies have reported that the leakage current density increases after PMA treatment [30,31], it is obvious that PMA can reduce the leakage current and enlarge the breakdown voltage significantly in our studies. Most of the samples remain un-breakdown when the electrical field is up to 2 MV/cm, except for the as-deposited sample and 400 °C/30 min treated one. In comparison with the 300 °C and 400 °C treated samples, the 350 °C processed one exhibits lowest leakage current (Fig. 6b), while the sample annealed for 30 min at this temperature shows the smallest leakage current density among all the durations (Fig. 6a). The leakage current density under the optimal condition of 350 °C/30 min, approaching 10^{-8} A/cm^2 at 1 MV/cm, reduces by three orders of magnitude compared to that of the as-deposited one. Fig. 7 is the plots of leakage current density at 1 MV/cm vs. various PMA conditions, which reveals the leakage current improvement after PMA treatment more directly.

For the leakage current reduction mechanism after PMA treatment, the hydrogen passivation model is adopted in this study, which is also reported elsewhere [14,15,32,33]. Y_2O_3 films, featuring high hygroscopicity in nature, are easily to absorb vapor in the air. Therefore, the hydroxyl groups (the water molecules are known to electrostatically dissociate into protons and hydroxyls) gathered at the Al/Y_2O_3 interface could react with the Al contact. Then the generated atomic H would diffuse into the dielectric and passivate the traps present at the interface or even in the bulk of Y_2O_3 films, making the defects that are responsible for the leakage current electrically inactive. The reaction can be described as follows:

$$x\mathrm{Al} + \mathrm{OH}^- + h^+ = \mathrm{AlO}_x + \mathrm{H}^+ + e^- \quad (7)$$

In comparison with the other PMA-treated samples, 350 °C treated one has the lowest leakage current. It is assumed that the lower treatment temperature cannot provide enough kinetic energy for hydrogen atoms to passivate the defects, while more higher PMA temperature would interfere the hydrogen passivation due to the decomposition of passivation center [15,33]. As to the result of 400 °C PMA in Fig. 6(b), there is another reason worthy to be mentioned. For a dielectric/substrate couple, a thermodynamically stable bonded interface, which is intrinsically linked to both dielectric and substrate, is important to maintain good adhesion and thus obtain good performance [34]. When PMA is undertaken at 400 °C, the ITO films are likely to get degraded and generate dangling bonds due to poor thermal stability [35]. This will introduce extra interface defects between Y_2O_3/ITO layers and finally deteriorate the electrical performance of MIM capacitors.

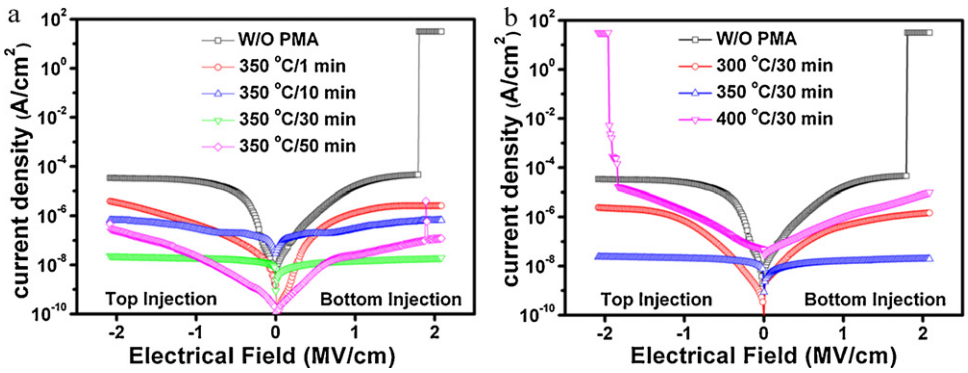

Fig. 6. Comparison of *J–E* characteristics of the samples at SP = 0.22 Pa with or without PMA (a) with different durations; (b) at different temperatures.

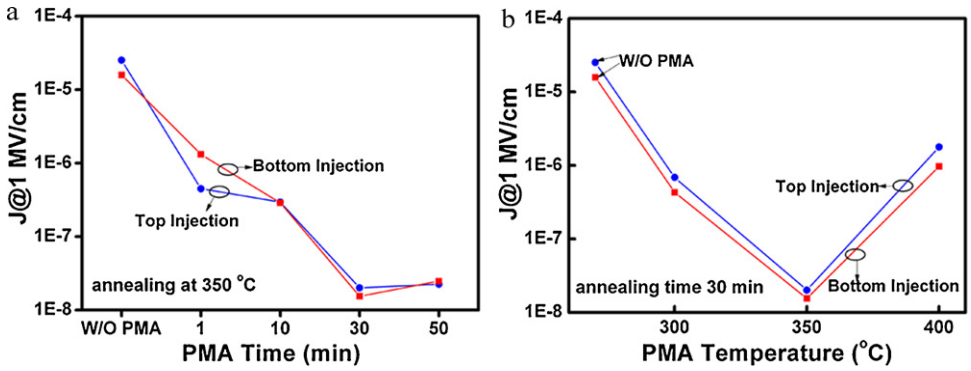

Fig. 7. The leakage current density at an applied field of 1 MV/cm for the samples (a) with various durations; (b) at various temperatures.

Furthermore, the leakage current mechanism is discussed to interpret the conduction behavior. The space-charge-limited current (SCLC) model has been developed to describe the current behavior of numerous thin films, such as organic materials, nitride, and rare earth oxides [25]. A plot of J vs. E^2 should be linear for SCLC mechanism as determined from Mott–Gurney Law [36]:

$$J = \frac{9}{8}\mu\varepsilon\varepsilon_0\frac{E^2}{L^3} \tag{8}$$

where μ is the free carrier mobility, ε is the dielectric constant of the material, E is the applied electrical field and L is the distance between two electrodes. It is clearly displayed in Fig. 8(a) that linear part fits well in most of the applied filed range, meaning the leakage current is dominated by SCLC mechanism for the as-deposited sample. It is generally considered high-k oxides have larger densities of trapped charges and interface states than SiO_2, causing more significant trap-induced current leakage. SCLC is such a typical mechanism responsible for the high trap density conduction [25].

As depicted in Fig. 8(b), the line extracted from the Schottky mechanism matches well with the PMA treated sample. The Schottky emission conduction can be expressed as [37]:

$$J = A * T^2 \exp\left[\frac{-q(\Phi_B - \sqrt{qE/4\pi\varepsilon_r\varepsilon_0})}{kT}\right] \tag{9}$$

For the Schottky emission, a plot of $\ln(J/T^2)$ vs. $E^{1/2}$ produces a straight line, and the fitted dynamic dielectric constant (i.e., the optical dielectric constant) can be obtained from the slope of the plot, which is equal to square of the refractive index ($\varepsilon_r = n^2$) theoretically [37,38]. In this study, the extracted ε_r is 2.61, of which the square root is close to the n value obtained by SE. So it is believed that the Schottky emission mechanism dominates the annealed films due to the reduction of traps such as vacancies and dangling bonds [39], which confirms the benefit of the H passivation arising from the PMA treatment.

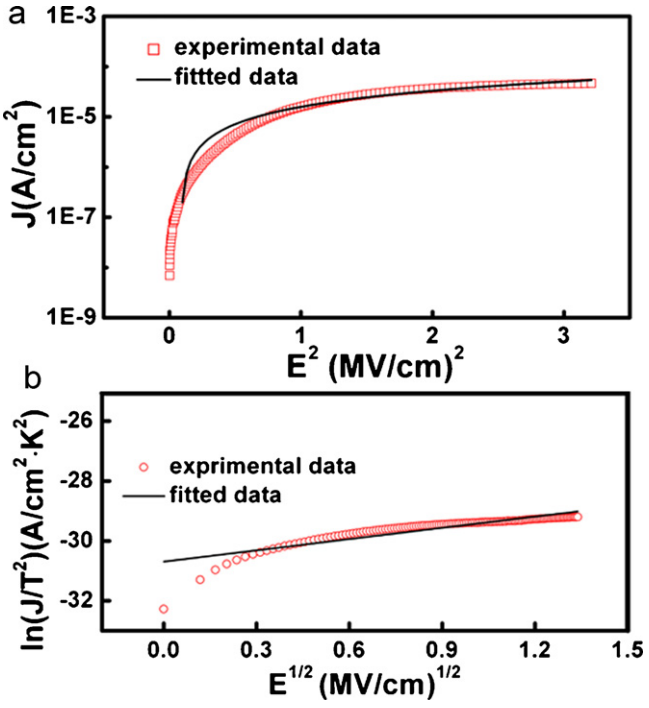

Fig. 8. Leakage current mechanism for the SP = 0.22 Pa, as-grown and SP = 0.22 Pa, 350 °C/30 min PMA treated samples (a) The plot of J vs. E^2 for the as-grown sample; (b) the plot of $\ln(J/T^2)$ vs. $E^{1/2}$ for the 350 °C/30 min PMA treated one.

4. Conclusions

In summary, the effects of sputtering pressure and low temperature post-metallization annealing (PMA) on the optical, structural and electrical performance of Y_2O_3 films were investigated. As the sputtering pressure decreases, it is found that the crystallinity is improved; meanwhile both the refractive index and band gap become larger but the leakage current density gets smaller due to the densification of the films. Post-metallization annealing treatment can significantly reduce the defects and enhance the electrical performance of Y_2O_3 films, which is thought to attribute to the atomic H making the defects at the interface or/and in the bulk of Y_2O_3 inactive. The space-charge-limited current model is found to fit well with the leakage current curve of the as-deposited films at most range, while the Schottky emission mechanism is found to well describe the leakage behavior of the PMA-treated samples.

Acknowledgements

The authors are grateful for the financial supports of the National Natural Science Foundation of China (grant no. 61076081), the Natural Science Foundation of Ningbo (grant no. 2010A610182), the key project of the Natural Science Foundation of Zhejiang province (grant no. Z4080347), Qianjiang Talent Program of Zhejiang Province (grant no. 2009R10072), the CAS/SAFEA International Partnership Program for Creative Research Teams, the aided program for Science and Technology Innovative Research Team of Ningbo Municipality (2009B21005), and the Special Foundation of President of the Chinese Academy of Sciences (grant no. 080421WA01).

References

[1] R. Navamathavan, C.K. Choi, S.J. Park, J. Alloys Compd. 475 (2009) 889.
[2] H.Z. Zhang, L.Y. Liang, A.H. Chen, Z.M. Liu, Appl. Phys. Lett. 97 (2010) 12.
[3] J.F. Wager, Science 300 (2003) 1245.
[4] W.H. Ha, M.H. Choo, S. Im, J. Non-Cryst. Solids 303 (2002) 78.
[5] X.R. Cheng, Z.M. Qi, G.B. Zhang, H.J. Zhou, W.P. Zhang, M. Yin, Phys. B 404 (2009) 146.
[6] E.K. Evangelou, C. Wiemer, M. Fanciulli, M. Sethu, W. Cranton, J. Appl. Phys. 94 (2003) 318.
[7] P.S. Das, G.K. Dalapati, D.Z. Chi, A. Biswas, C.K. Mati, Appl. Surf. Sci. 256 (2010) 2245.
[8] L. Shi, Y. Zhou, J. Yin, Z.G. Zhou, J. Appl. Phys. 107 (2010) 1.
[9] K. Wasa, M. Kitabatake, H. Adachi, Thin Flim Materials Technology, Springer, 2004.
[10] Y.Y. Liu, L.Q. Qian, C. Guo, X. Jia, J.W. Wang, W.H. Tang, J. Alloys Compd. 479 (2009) 532.
[11] R. Ohnishi, M. Katayama, K. Takanabe, J. Kubota, K. Domen, Electrochim. Acta 55 (2010) 5393.
[12] I. Kim, S.K. Han, C.M. Osburn, J. Electrochem. Soc. 151 (2004) F29.
[13] M. Yun, M.S. Kim, Y.D. Ko, T.H. Moon, J.H. Hong, J.M. Myoung, I. Yun, Microelectron. Eng. 77 (2005) 48.
[14] K.T. Lee, C.F. Huang, J. Gong, B.H. Liou, IEEE Electron. Device Lett. 30 (2009) 907.
[15] E.H. Nicollian, J.R. Brews, MOS (Metal Oxide Semiconductor) Physics and Technology, Wiley, 1982.
[16] X.J. Wang, L.D. Zhang, G. He, J.P. Zhang, M. Liu, L.Q. Zhu, J. Appl. Phys. 103 (2008) 64101.
[17] A. Dimoulas, A. Travlos, G. Vellianitis, N. Boukos, K. Argyropoulos, J. Appl. Phys. 90 (2001) 4224.
[18] X.J. Wang, L.D. Zhang, G. He, L.Q. Zhou, M. Liu, J.P. Zhang, J. Phys. D 42 (2009) 215405.
[19] Y. Guyot, R. Moncorge, L.D. Merkle, B. Mclntosh, H. Verdun, Opt. Mater. 5 (1996) 127.
[20] Y.-B. Chen, C.-L. Huang, S.-H. Lin, J. Alloys Compd. 480 (2009) 897.
[21] B.E. Yoldas, Appl. Opt. 19 (1980) 1425.
[22] X.J. Wang, L.D. Zhang, J.P. Zhang, Mater. Lett. 62 (2008) 4235.
[23] L.Q. Zhu, Q. Fang, M. Liu, G. He, L.D. Zhang, Appl. Surf. Sci. 254 (2008) 5439.
[24] H. Hu, C.X. Zhu, Y.F. Lu, T. Liew, B.J. Cho, W.K. Choi, N. Yakovlev, J. Appl. Phys. 94 (2003) 551.
[25] Y.S. Kim, S.I. Ohmi, K. Tsutsui, H. Iwa, Jpn. J. Appl. Phys. Part 1 44 (2005) 4032.
[26] R.H. Horng, D.S. Wuu, J.W. Yu, C.Y. Kung, Thin Solid Films 289 (1996) 234.
[27] T. Tolke, A. Kriltz, A. Rechtenbach, Thin Solid Films 518 (2010) 4242.
[28] Y.-B. Chen, C.-L. Huang, Surf. Coat. Technol. 201 (2006) 654.
[29] F. Lai, L.M. Lin, Z.G. Huang, R.Q. Gai, Y. Qu, Appl. Surf. Sci. 253 (2006) 1801.
[30] E. Atanassova, D. Spassov, Microelectron. J. 30 (1999) 265.
[31] J.S. Lee, Y. Li, S.Y. Lee, Q.X. Jia, Appl. Phys. Lett. 84 (2004) 3825.
[32] W.S. Lau, K.K. Khaw, T. Han, N.P. Sandler, Appl. Phys. Lett. 89 (2006) 262901.
[33] C.C. Huang, C.H. Cheng, K. Lee, B.H. Liou, Electrochem, Solid State Lett. 12 (2009) H123.
[34] J. Lin, T. Suzuki, D. Matsunaga, K. Eguchi, Appl. Phys. Lett. 88 (2006) 062902.
[35] G. Eftekhari, J. Vac. Sci. Technol. B 13 (1995) 1560.
[36] P.N. Murgatro, J. Phys. D 3 (1970) 151.
[37] F.C. Chiu, Electrochem, Solid State Lett. 11 (2008) H135.
[38] K.H. Cho, C.H. Choi, J.Y. Choi, T.G. Seong, S. Nahm, C.Y. Kang, S.J. Yoon, J.H. Kim, J. Eur. Ceram. Soc. 30 (2010) 513.
[39] J.Y. Tewg, Y. Kuo, J. Lu, B.W. Schueler, J. Electrochem. Soc. 151 (2004) F59.